International Journal of Multiphase Flow 113 (2019) 250–263

Contents lists available at ScienceDirect

International Journal of Multiphase Flow

journal homepage: www.elsevier.com/locate/ijmulflow

Characteristics of churn and annular flows in a large diameter vertical riser

M. Abdulkadir[a,*], U.P. Mbalisigwe[a], D. Zhao[b], V. Hernandez-Perez[c], B.J. Azzopardi[d], S. Tahir[e]

[a] Department of Chemical Engineering, Federal University of Technology, Minna, Niger State, Nigeria
[b] School of Engineering, London South Bank University, London, United Kingdom
[c] Department of Mechanical Engineering, Faculty of Engineering, National University of Singapore, Singapore
[d] Process and Environmental Engineering Research Division, Faculty of Engineering, University of Nottingham, University Park, Nottingham NG7 2RD, United Kingdom
[e] Department of Economics, Faculty of Social Sciences, Usmanu Danfodio University, Sokoto, Nigeria

ARTICLE INFO

Article history:
Received 13 August 2018
Revised 25 November 2018
Accepted 31 January 2019
Available online 1 February 2019

Keywords:
Film fraction
Churn–annular flow
Entrance length
Structure velocity
Frequency
Waves

ABSTRACT

This paper presents the results of a series of experimental studies conducted to investigate the characteristics of churn and annular flows in an 11 m long riser with the internal diameter of 127 mm. A series of experiments in churn–annular flow regime were performed for a range of gas superficial velocities (3.5–16.1 m/s) and liquid superficial velocities of 0.02–0.33 m/s. Statistical analysis involving average, standard deviation and skewness, dominant frequency and structure velocity of the time series data was carried out as a quantitative approach to discriminate between churn and annular flows and to describe the transition between them. The variation of average liquid film thickness against gas superficial velocity showed a minimum at gas superficial velocity of 12.4 m/s. This is in close agreement with the minima at gas superficial velocity of 13 m/s reported in the literature. The results of the comparison between average liquid film thicknesses from the conductance ring probes agree well with those obtained by using local liquid film thickness probes and conductance ring probes in the literature. The results of the comparison of dominant frequency obtained from the conductance ring probes agree well with those obtained by using wire mesh sensor (WMS) in the literature. A comparative analysis of the current experimental data with those previously published experimental results confirms good agreement.

1. Introduction

In the petroleum industry, two-phase gas–liquid flow occurs in flowlines, risers, gas production systems and well tubing. Large diameter pipes are often encountered in offshore production systems involving large diameter risers connecting the seabed to a platform or floating production, storage and offloading (FPSO) units. Large diameter risers can also be employed during the simultaneous transportation of gas and liquid phases over a long distance where the diameter of the pipe according to Sharaf et al. (2016) is $\geq$ 75 mm and its length according to Waltrich et al. (2013) is of the order of thousands of pipe diameter before phase separation. Consequently, this raises questions about the characterisation of churn and annular flows since it may eventually lead to transitions between the ensuing flow patterns. It is worth mentioning that this characterisation has vital practical applications in the oil and gas industry. Unfortunately, much of the published work on the characteristics of churn and annular flow patterns concentrates on pipes with small internal diameter, 9–55 mm (Brown et al., 1975; Wolf et al., 2001; van Hout et al., 2001; Barbosa et al., 2001; Hazuku et al., 2008; Kaji et al., 2009; Da Riva and Del Col, 2009; Julia et al., 2009; Wang et al., 2012 and Waltrich et al., 2013). Furthermore, the developments in a number of industries, from heat exchangers to large internal diameter deep water risers require the need for the knowledge of multiphase flow in larger diameter pipes, in which the flow behaviour may be significantly different from that in smaller diameter pipes.

The research on large diameter pipes is rare due to its challenging requirement. It entails high pumping power and long pipe for flow development. When data are required for the design of large diameter systems, engineers have to extrapolate the data obtained in small diameter pipes. Many studies however show that the data obtained in such manner possessed uncertain errors due to the complexity arising from gas–liquid two phase interactions. This can be attributed to inadequate understanding of the complicated flow

* Corresponding author.
E-mail address: mukhau@futminna.edu.ng (M. Abdulkadir).

https://doi.org/10.1016/j.ijmultiphaseflow.2019.01.013
0301-9322/

Nomenclature

D	pipe diameter (mm)
De	distance between pair of electrode plates (mm)
s	electrode width (mm)
De/D	electrode spacing to pipe diameter ratio
s/D	electrode width to pipe diameter
Ge^*	dimensionless conductance
L/D	dimensionless axial location
U_{SL}	liquid superficial velocity (m/s)
U_{SG}	gas superficial velocity (m/s)
Um	mixture velocity (m/s)
U_G	actual gas velocity (m/s)
U_L	actual liquid velocity (m/s)
Vgd	drift velocity (m/s)
d	drift coefficient
C_0	flow distribution parameter
g	acceleration due to gravity (m/s^2)
U_R	slip ratio
M_l, M_g	liquid and gas mass fluxes (kg/m^{2}s), respectively
A	cross sectional area (m^2)
x	gas quality
p_{atm}	atmospheric pressure (bar)
p_{system}	system pressure (bar)
S	standard deviation of film fraction
Sk	skewness of film fraction
PSD	power spectral density
T	time series period (seconds)
N	number of data points in the time series
ρ_l, ρ_g	liquid and gas densities (kg/m^3), respectively
θ	inclination angle of the pipe
σ	surface tension (N/m)
ε	void fraction
ε_L	film fraction

behaviour in large diameter pipes (Kataoka and Ishii, 1987 and Ohnuki et al., 1995). The unsatisfactory results from industrial applications have led to researchers questioning the validity of such extrapolation. Thus, further research on larger diameter pipes is needed to better understand the scale of the problems.

The major motivation of this work is to expand the rather scant availability of experimental data for large diameter pipes. It primarily focuses on churn–annular flow which is particularly relevant to gas–oil transportation in pipelines.

2. Literature review

2.1. Gas–liquid flow in large diameter pipes

Omebere-Iyari and Azzopardi (2007), Ali (2009), Van der Meulen (2012) and Zabaras et al. (2013) have attempted to investigate the behaviour of two-phase flow in large diameter ($D \geq 127$ mm) vertical pipes. Some of these studies concerned with large diameter pipes showed experimentally that churn flow is commonly observed over a wide range of gas and liquid velocities. They also observed, more importantly, that the behaviour of gas–liquid flow patterns is significantly different in larger diameter pipes in comparison to smaller pipes. For instance, slug flow was not observed in large pipe diameters when it was expected to occur in smaller diameter pipes at the same flow conditions.

According to SPE (2015) the use of multiphase flow models for large diameter ($D \geq 100$ mm) pipes is essential for the calculation of Worst Case Discharge (WCD) for offshore wells. They claimed that the extension of existing mechanistic models and flow correlations, built based on experiments conducted using small diameter pipes however, is still unreliable. They concluded that further research on the behaviour of multiphase flows in large diameter pipes is vital and that correlations applicable at high flow rates in large diameter pipes are needed. Zabaras et al. (2013) also argued on the need for two-phase flow models obtained from large diameter pipes for gas-lift applications within offshore risers.

In a comprehensive review on annular flow and its modelling, Azzopardi (1997) reported, the majority of available experimental data on disturbance wave properties were obtained using small diameter pipes and at near atmospheric pressure conditions. In addition, very few of published papers on churn and annular flows were obtained for liquid superficial velocity beyond 0.1 m/s and several of the previous experimental studies employed subjective methods for the estimation of these properties (Azzopardi, 1986). Therefore, further studies are required to clarify the detailed characteristics of churn–annular flow in large diameter pipes at above atmospheric pressure and using more objective statistical analysis methods.

2.2. Churn–annular gas–liquid flows behaviour

Brown et al. (1975) experimentally investigated the flow development leading to hydrodynamic equilibrium in annular flow in heated and unheated vertical 9.61 mm diameter pipes. They observed that the wave spectrum took fairly long distances to develop.

According to Hewitt et al. (1985), in churn flow, large waves are typically created on the liquid film due to the drag force exerted by the gas phase flowing upwards at a velocity higher than the net-upward liquid film velocity. They concluded that large waves frequently break up and a large fraction of the liquid can be entrained as droplets or lumps of liquid. Upstream to the large liquid film waves, a thin liquid film flows downward, and part of this film is carried upwards by subsequent large waves flowing upwards.

Sekoguchi and Takeishi (1989) reported that as the liquid flow rate increased at a given gas velocity, wispy annular flow is observed. They, however, failed to establish a transitional boundary between the regular annular flow and wispy annular flow. Eleven years later, Hawkes et al. (2000) reproduced the annular flow studies of Sekoguchi and Takeishi (1989) and reported similar observations.

According to Jayanti and Hewitt (1992) churn flow is regarded as a transition between slug and annular flow. They observed that a direct transition from slug or even from bubbly flow directly to annular flow may happen at very high liquid flow rates. Some researchers like Mao and Dukler (1993) do not recognise churn flow as a separate flow pattern because of its similarity to annular flow. Many other researchers believe that this flow pattern is simply a transition regime. For instance, Taitel et al. (1980) and Dukler and Taitel (1986) describe churn flow as an entrance phenomenon preceding a downstream stable slug flow for a pipe of enough length.

As far as churn flow is concerned, Hewitt and Jayanti (1993), Jayanti et al. (1993), Azzopardi and Wren (2004) and Waltrich et al. (2013) confirmed its existence as a separate flow pattern. Many investigators like Govier and Aziz, 1972 Oshinowo and Charles, 1974, Taitel et al., 1980 and Mishima and Ishii (1984) have identified the existence of churn flow based on visual observation of gas–liquid flow in transparent tubes and from the study of simple conductance probe time series.

According to Ansari et al. (1994) and Shoham (2006), churn flow is a very chaotic flow pattern. They also affirmed that the physics of this flow pattern is very difficult to model and describe owing to its complexity. According to Barbosa et al. (2001), churn flow is similar to annular flow in that liquid films are present around the pipe wall and a large gas core is positioned in the mid-

dle of the pipe. However, in churn flow, the liquid film flows in an oscillatory manner, upwards and downwards based on the fact that the gas velocity is not high enough to levitate the liquid continuously.

Barbosa et al. (2001) and Wang et al. (2012) investigated flow development and wave behaviour in churn flow. However, their work was limited to the region near the entrance. Hazuku et al. (2008) measured the evolution of liquid film thickness and wave characteristics in a vertical 3 m long with 11 mm diameter pipe by means of a laser focus displacement technique. They concluded that the flow did not reach a developed state in the test section based on the fact that neither the liquid film thickness nor the wave frequency ceased to decrease as a function of distance.

Wang et al. (2012) developed a model for predicting the movement of huge waves. They claimed that when the gas superficial velocity increases the wave amplitude decreases. Sharaf et al. (2016) investigated the structures in gas–liquid churn flow in a large 127 mm internal diameter and 11 m long pipe using conductance wire mesh sensor (WMS). They extracted the time series data from the WMS output and examined the trends of mean liquid film thickness, base film and wave peaks. They qualitatively examined the occurrence of wisps and their corresponding frequency. However, they did not report annular flow and did not fully characterise churn and annular flows which have vital practical application in the oil and gas industry.

From the studies regarding the characteristic of churn and annular flows, there emerges a clear need for more experimental data on the evolution of gas–liquid flows in vertical pipes with larger pipe diameters. This work therefore aims to experimentally investigate the characteristics of periodic structure behaviour of film fraction at a pressure of 3 bar (a). It will focus on liquid superficial velocity of 0.02–0.33 m/s within the churn–annular flow in a 127 mm internal diameter and 11 m long vertical riser using air–water as the system fluid.

3. Experimental arrangement

3.1. Experimental facility

The present experimental programme was carried out using a large close loop facility shown schematically in Fig. 1. The facility is located within the Chemical Engineering Laboratories of the University of Nottingham. It has been reported previously by Abdulkadir et al. (2012, 2014). The technical details can be found in the reported papers. However, for sake of comprehensiveness, a brief description of the facility is presented here. The facility works as follows: the liquid (water) is stored in the supply tank and is transported by means of a centrifugal pump into the mixer positioned at the base of the riser. Two liquid ring pumps with 55 kW motors were employed to compress and transport the air to the mixer. The mixing device (Fig. 1F) consists of a 105 mm diameter tube sited at the centre of the 127 mm internal diameter test section, called an annular injection method. Air and water meet in the mixer and afterwards begin its development along the length of the 11 m high riser. The flow is then directed into the downcomer

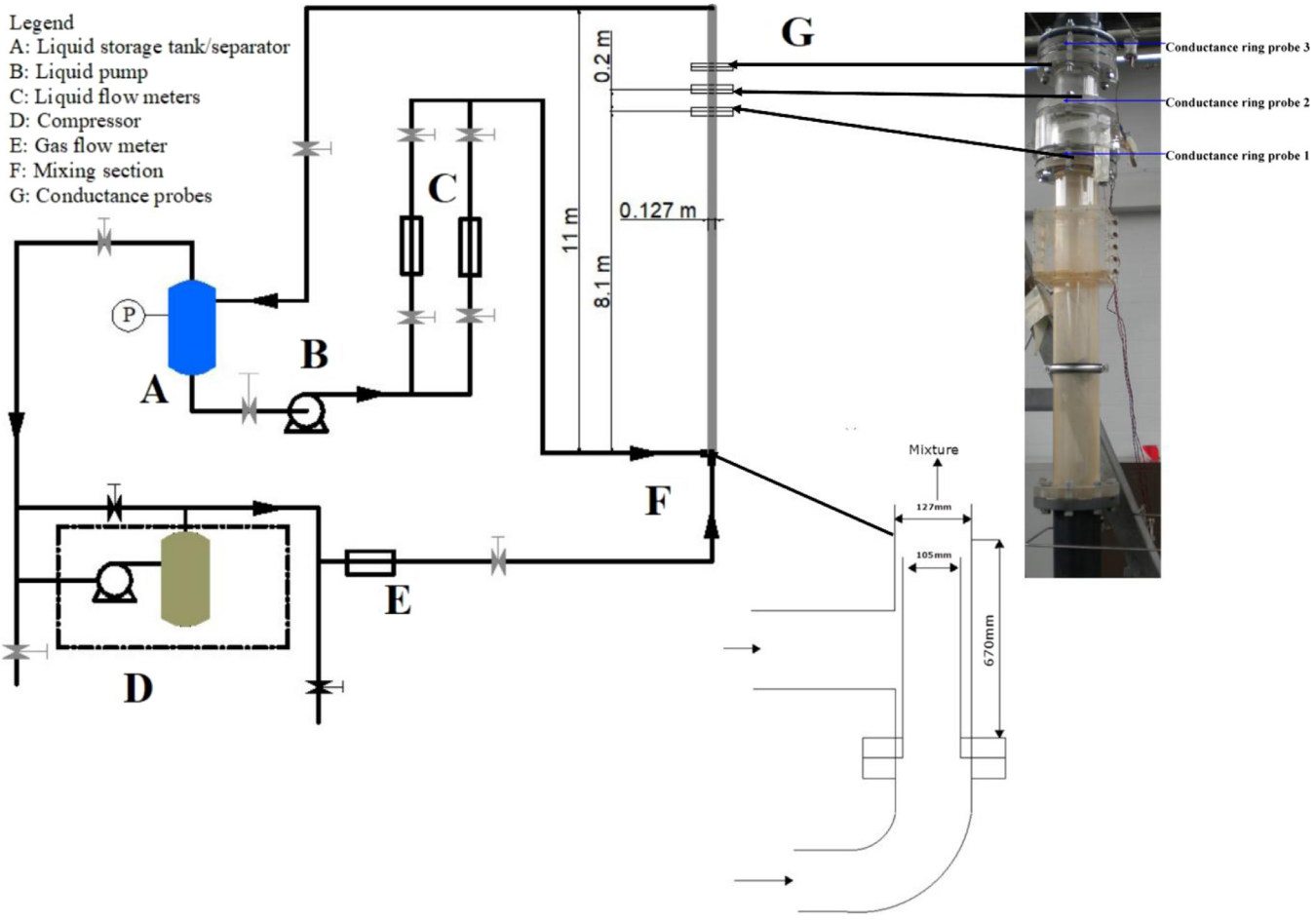

Fig. 1. Schematic diagram of the experimental facility showing (A) liquid storage tank (B) liquid pump (C) liquid flow meters (D) compressor (E) gas flow meter (F) air–water mixing section and (G) the locations of the conductance probes on the transparent test section of the riser.

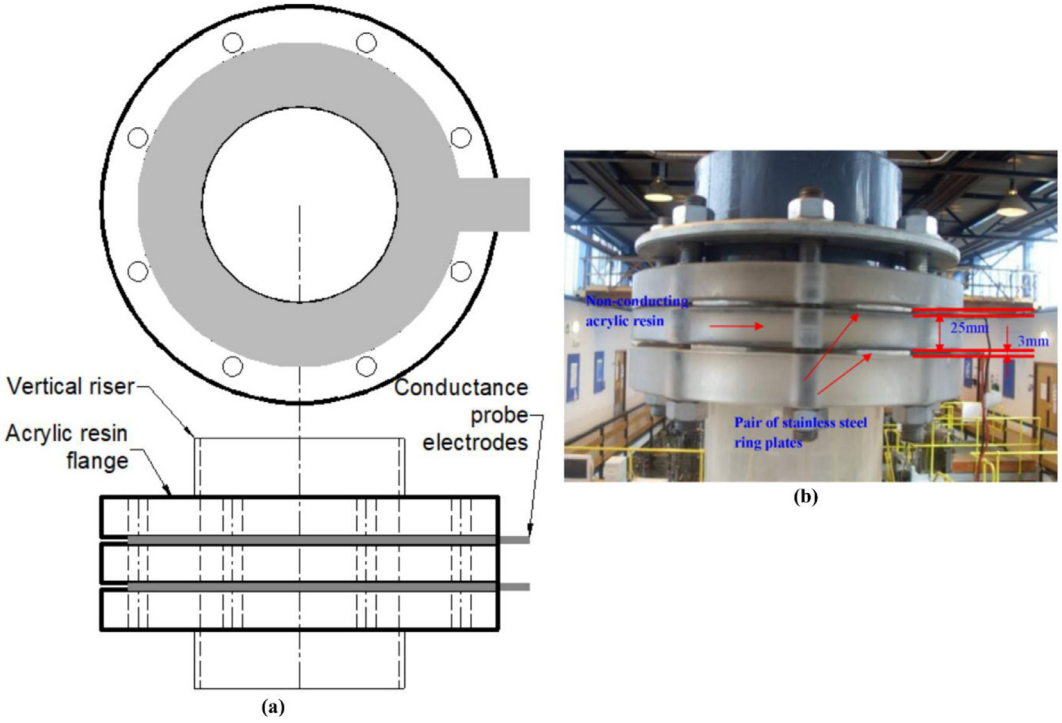

Fig. 2. The conductance ring probes.

which is linked to the supply tank where the liquid is separated from the gas. The flow rates of the air and water are controlled by valves and measured using calibrated vortex and turbine meters, respectively. The maximum uncertainties in the liquid and gas flow rates according to Sharaf et al. (2016) are ±0.6% and ±0.5%, respectively.

The pressure and temperature of the system were taken close to the liquid and gas flow meters and at the base of the riser. This permitted the inlet flow rates to the test section for both phases to be determined precisely. The liquid and gas superficial velocities employed were in the ranges from 0.02 to 0.33 m/s and 3.5 to 16.1 m/s, respectively. In all of the experiments, air and mains tap water at a temperature of 20 °C were used as the test fluids. The experiments were carried out at a system pressure of 3 bar(a). This system pressure corresponds to a gas density of 3.55 kg/m^3.

Downstream of the mixer, the two-phase mixture travels for 11 m along a 127 mm internal diameter vertical pipe in which annular or churn flow is established. Here, the time varying cross-sectional film fractions were measured using three identical conductance ring probes Fig. 1(G) placed at distances of 8.1, 8.3 and 8.5 m above the mixer section. These locations correspond to, 64, 65 and 67 pipe diameters above the mixer. Beyond the vertical pipe test section, the two-phase flow travels for 2.34 m horizontally, a further 9.67 m vertically downwards and 1.47 m horizontally to the separator.

3.2. Instrumentation

3.2.1. Film fraction measurement

In the present study the conductance technique is applied to study air–water distribution. Air–water mixtures were considered. An alternating current carrier voltage of 10 kHz frequency was applied across each pair of electrodes while an electronic device, exclusively designed for this purpose, changed the alternating current signal into a direct current signal proportional to the impedance of the two-phase test section. The authors found that the frequency of 10 kHz is high enough to ensure the measured electrical impedance is resistive. The frequency was verified to give the resistive behaviour of the water by measuring both the amplitude and phase shift of the applied voltage signal.

3.2.1.1. Conductance ring probe technique. The design of the conductance ring probes as used in the present study was painstakingly described by Omebere-Iyari (2006). The flush mounted ring probes shown in Fig. 2 are attractive to researchers based on the fact that it provides non-intrusive measurements, can detect small impedance and allows electric field to be effectively confined.

In the present study, it is worth mentioning that the probes must be calibrated before the beginning of measurement. This according to Fossa (1998) is to ensure better accuracy. The probes employed in this work were calibrated by Omebere-Iyari (2006) for bubble, churn and annular flow regimes. The churn and annular flows are simulated by inserting a non-conducting cylindrical plastic rod with a known diameter inside the pipe and filling the annulus between the rod and the pipe wall with a conductive liquid. The probes give an output ranging from 0 to 0.32 V, which is proportional to the resistance of the air–water mixture. They were cautiously designed so that the electrodes had the same diameter, D as the test section (127 mm) to guarantee flush mounting with the pipe wall. The distance between each pair of stainless steel electrode plates, D_e, and width, s, are 25 and 0.3 mm, respectively. The distances, D_e and s can be observed in Fig. 2. This results in electrode spacing to pipe diameter ratio (D_e/D) of 0.20 and electrode width to pipe diameter ratio (s/D) = 0.024 (Abdulkadir et al., 2012). By repeating this procedure with plastic rods of different diameters according to Abdulkadir et al. (2012), void fraction/dimensionless conductance relationship were obtained. Data acquisition was carried out through a PC equipped with a National Instrument (NI) DAQ card. An existing data acquisition programme in Labview (Omebere-Iyari, 2006) was adapted. A third order polynomial fit of the form:

$$\text{Film fraction} = a + b(Ge*)^3 + c(Ge*)^2 + d(Ge*) \quad (1)$$

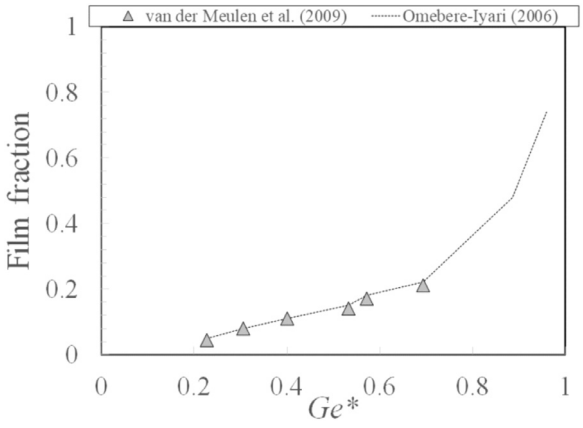

Fig. 3. Calibration relationships for conductance ring probes for churn–annular type flow.

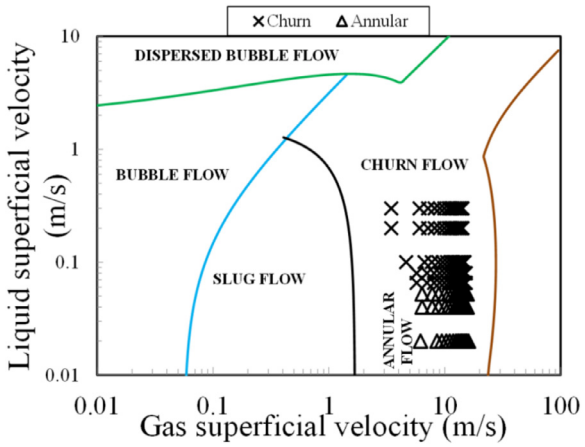

Fig. 4. Flow pattern map under current experimental conditions predicted by Pereyra and Torres (2005).

is used to obtain a distinctive calibration curve for each probe. It is worthy of mention that Van der Meulen (2012) much later, following the same procedure re-calibrated the probes wherein the effect of gas bubbles in the liquid film was taken into consideration. Van der Meulen (2012) successfully simulated the gas bubbles in the liquid film by adding a known volume of spherical glass beads with different diameters ranging from 3 to 6 mm to the annulus between the non-conducting rod and the pipe wall. Details on the role of the glass beads during calibration can be found in Van der Meulen (2012).

Fig. 3 shows the calibration curves for churn and annular flow types for the approaches of Omebere-Iyari (2006) and Van der Meulen (2012). Time varying cross-sectional film fraction measurements was made with three identical ring probes at three locations along the length of the riser.

In conclusion, tap water, which was used in the experiments, was found to have conductivity between 491 and 600 μScm^{-1}. If not replaced the water quickly became contaminated and mineral deposits begun to show, mostly on the wires. To avoid large variations of conductivity within the same experimental run and to reduce fouling of the electrodes, fresh water was fed continuously to the separator tank and discharged to drain. The conductivities determined during the measurement were used to interpolate between the calibrations curves to obtain the liquid film thickness relationship. Calibrations were repeated periodically without a cleaning of the electrodes. It was observed that the variations of the calibration curves caused changes in the film fraction, which were well within experimental error. The largest discrepancy recorded was 4.5%. In addition, one of the pitfalls of the conductance probes was that the liquid conductivity varies with temperature. The problem was solved by keeping the temperature constant during the experiment.

4. Results and discussion

The range of liquid and gas superficial velocities is given in Table 1. In total, 136 data points were obtained during the test runs for all the experimental conditions. Fig. 4 shows the experimental operating points of the present study described in a flow pattern map (Fig. 4) generated using the FLOPATN computer code developed by Pereyra and Torres (2005). They used the model of Barnea (1987) for the transition criteria between different two-phase flow regimes. From an analysis of the observations it is concluded that the Pereyra and Torres (2005) model under-predicts annular flow, it predicts both churn and annular flows as churn flow.

The time series output of the 3 conductance ring probes gave the footprint of film fraction in the riser. By statistically analysing these data, the characteristic features of the flow behaviour such as average film fraction, film roughness reflected by the standard deviation of film fraction, skewness of film fraction, dominant frequency and structure velocity can be derived. Statistical analysis provides a quantitative tool to distinguish different flow patterns and to reveal the transition from one to another. The results are presented below.

4.1. Time series of film fraction

Fig. 5(a–c) presents the experimental results of film fraction as a function of time obtained from three conductance probes placed at three dimensionless axial distances L/D = 64, 65 and 67 and for gas superficial velocities of 3.5 and 16.1 m/s. It is worthy of mention that the experiment was repeated three times to check for repeatability and consistency. As can be seen, the film fraction decreases with an increase in gas superficial velocity. The oscillatory nature, large wave height and high film fraction that are characteristics features of churn flow become more evident at the low gas superficial velocity of 3.5 m/s. Similar trend has also been reported by previous investigators such as Almabrok (2013). At gas superficial velocity of 16.1 m/s, it can be seen from the figure that the peak of the film fraction decreases by about 60% for all the three dimensionless axial locations considered. It can also be observed that large amplitude variations cease to exist as gas superficial velocity increases to 16.1 m/s. This is in agreement with the observations of Wang et al. (2013) that when the gas superficial velocity increases, the wave amplitude decreases. At gas superficial velocity

Table 1
The range of variables.

U_{SG} (m/s)	U_{SL} (m/s)	Film fraction	Absolute error	Relative error (%)	Re_{SG}	Re_{SL}
3.5–16.1	0.02–0.33	0.05–0.2	0.018–0.027	1.8–5	86,413–402,000	2535–41,826

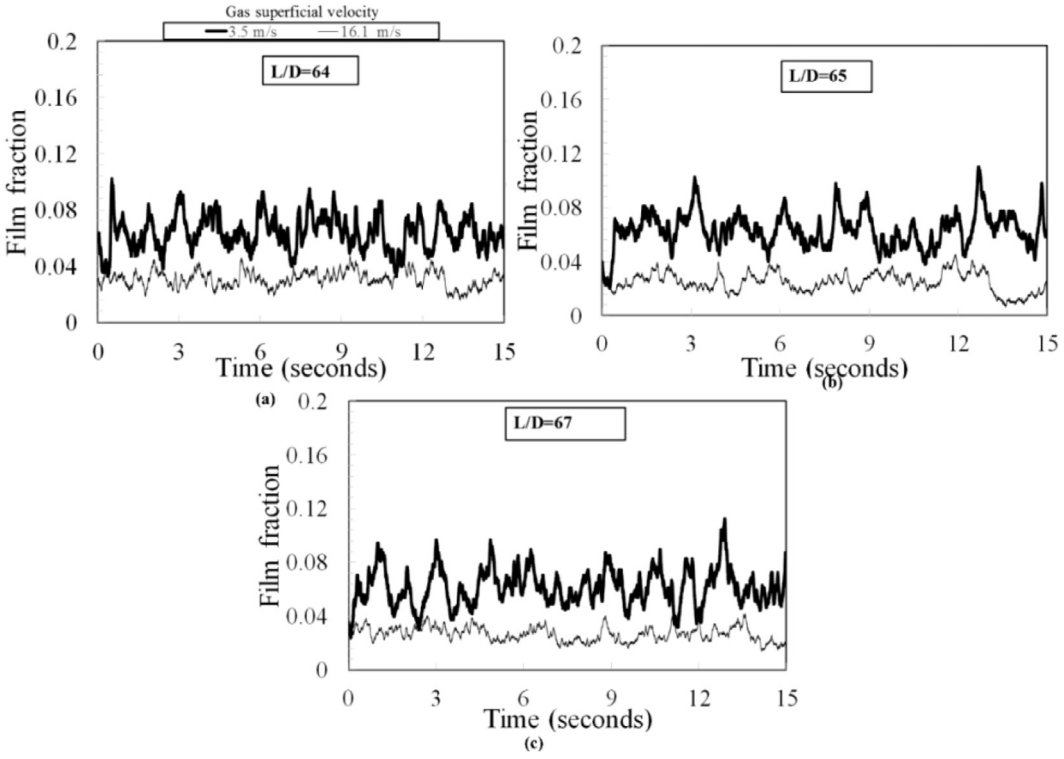

Fig. 5. A plot of time series of film fraction at L/D = 64, 65 and 67 at gas superficial velocities of 3.5 and 16.1 m/s. The liquid superficial velocity is 0.05 m/s.

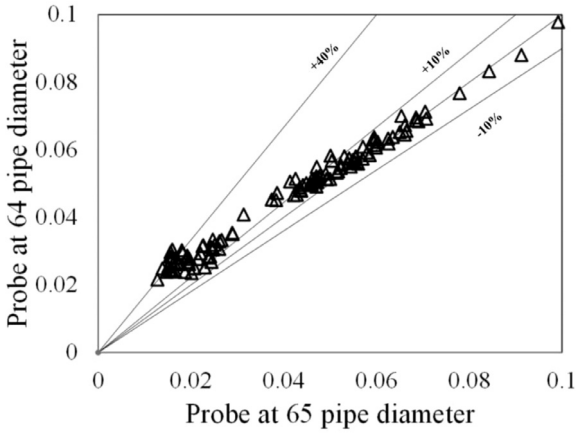

Fig. 6. Comparison of experimental film fraction data obtained at L/D = 64 and 65.

of 16.1 m/s, the time series shows a very low average value of film fraction. These are representative characteristics of annular flow.

The observed trend in the time series of film fraction as depicted in Fig. 5(a) shows a minor difference in comparison to Fig. 5(b–c). Fig. 5(b) shows almost the same trend in the variation of film fraction with respect to time in comparison to Fig. 5(c).

Fig. 6 shows a comparison of average film fraction obtained from two conductance probes placed at two dimensionless axial locations L/D = 64 and 65. The result from the film fraction data presented in Fig. 6 shows that most of the data from the two dimensionless axial locations agree well with each other and lie on a straight line. Similar trend was observed by Omebere-Iyari (2006) and Abdulkadir et al. (2012) at L/D = 64 using the same pipe diameter.

The result of the comparison depicted in Fig. 6 shows that for film fraction ≤ 0.04, there is a noticeable over-departure within +40%. An error of $\pm 10\%$ is achieved for $0.04 \leq$ film fraction ≤ 0.1.

4.2. Average film fraction

The average film fraction can be obtained from Eq. (2);

$$\langle \varepsilon_{kT} \rangle = \frac{1}{T}\int_T \varepsilon_k dt = \frac{1}{N}\sum_{n=1}^{n=N} \varepsilon_k \tag{2}$$

$\langle\rangle_T$ represents the average over the entire time series period (T) and N stands for the number of data points in the time series.

The average film fraction calculated using Eq. (2) from the time series data obtained from the conductance probes is plotted against gas superficial velocity as shown in Fig. 7.

The data is obtained for a series of liquid and gas superficial velocities of (0.02–0.2) m/s and (3.5–16.1) m/s, respectively. The figure illustrates that the average film fraction depends on both the gas and liquid superficial velocities. It is also clear from the plot that the average film fraction generally decreases with gas superficial velocity for all the liquid superficial velocities considered.

Fig. 7(a-b) shows that for liquid superficial velocity ranging from 0.02 to 0.05 m/s, the slope of the points is higher at gas superficial velocity up to about 8.0 m/s after which, the average film fraction remains relatively uniform at higher gas superficial velocities. The relative uniformity of average film fraction may be as a result of annular flow regime existing at higher gas superficial velocities. According to Azzopardi (1986), disturbance waves become more regular and reach more uniform velocity when the waves become very close to each other without coalescence of the successive waves. A similar trend in the plot of average film fraction with gas superficial velocity can be observed at liquid superficial velocities of 0.07 and 0.2 m/s. Although, the average value of film fraction for liquid superficial velocity of 0.2 m/s is always higher than that for liquid superficial velocity of 0.07 m/s.

A similar trend can be observed at liquid superficial velocities of 0.07 and 0.08 m/s. At liquid superficial velocity of 0.08 m/s, the film fraction decreases with gas superficial velocity. This decrease signifies smoothing of the interface and also a thinning of the film.

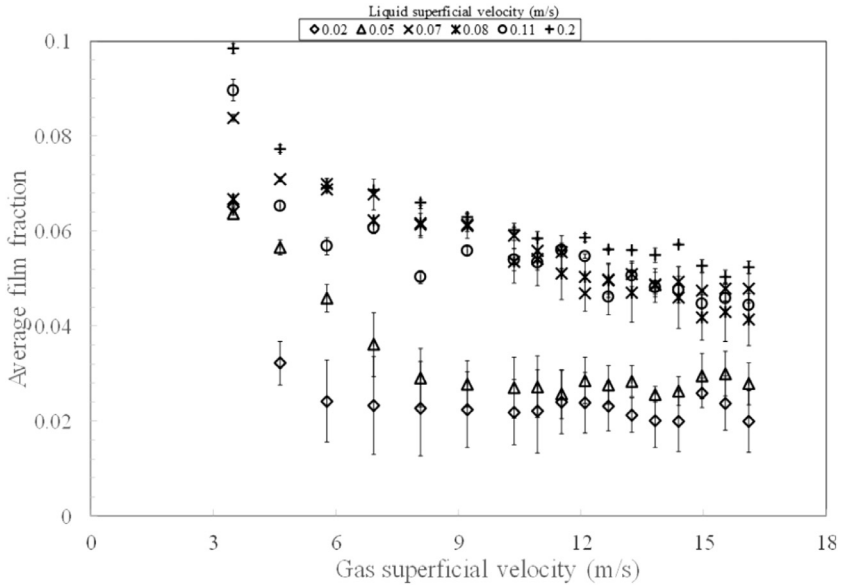

Fig. 7. A plot of variation of average film fraction with gas superficial velocity at various liquid superficial velocities. The error bar represents standard deviation.

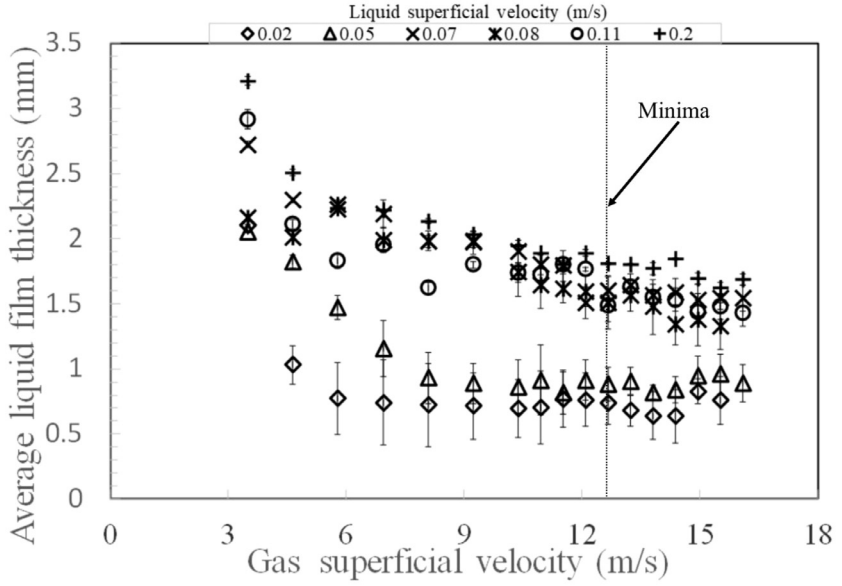

Fig. 8. Variation of average liquid film thickness with gas superficial velocity at liquid and gas superficial velocities of 0.02–0.2 m/s and 3.5–16.1 m/s, respectively. The error bar represents standard deviation.

At higher liquid superficial velocity of 0.1 m/s, the film fraction decreases from 0.096 to 0.056. It thereafter recovered to 0.062 and then decreased finally to 0.038. The decrease could be attributed to the thinning of the interface due to the action of interfacial shear stress leading to thinning of the film. The increase on the other hand can be attributed to the presence of liquid entrainment in the gas core and as a consequence brining about thickening of the film.

At liquid and gas superficial velocities of 0.2 and 3.5 m/s, respectively, a maximum film fraction of 0.1 can be seen in Fig. 7f. When the liquid superficial velocities are 0.08 and 0.1 m/s, there is a continuous decrease in average film fraction as the gas superficial velocity increases. This decrease could be attributed to the presence of churn flow within the range of gas and liquid superficial velocities considered. An interesting feature that can be deduced from Fig. 7(a–f) is that the peak value of film fraction occurred at the lowest gas superficial velocity except for liquid superficial velocity of 0.08 m/s where the peak film fraction is seen at 6.0 m/s. From the result, it can be observed that the liquid and gas superficial velocities have considerable effect on the film fraction, although to a varying degree. Also, the film fraction decreases more rapidly at lower gas superficial velocity up to a point and then remain steadily uniform at higher gas flow rates, similar observations were reported by Abdulkadir et al. (2012) and Almabrok (2013).

4.3. Liquid film thickness

The liquid film thickness is calculated from film fraction using Eq. (3). Similar method has been used by Kaji and Azzopardi (2010), Van der Meulen (2012), Zangana (2011) and Abdulkadir et al. (2012). The calculated liquid film thickness is then plotted against gas superficial velocity. This can be found in Fig. 8.

$$\delta = \frac{D}{2}\left[1 - (1 - \varepsilon_L)^{0.5}\right] \tag{3}$$

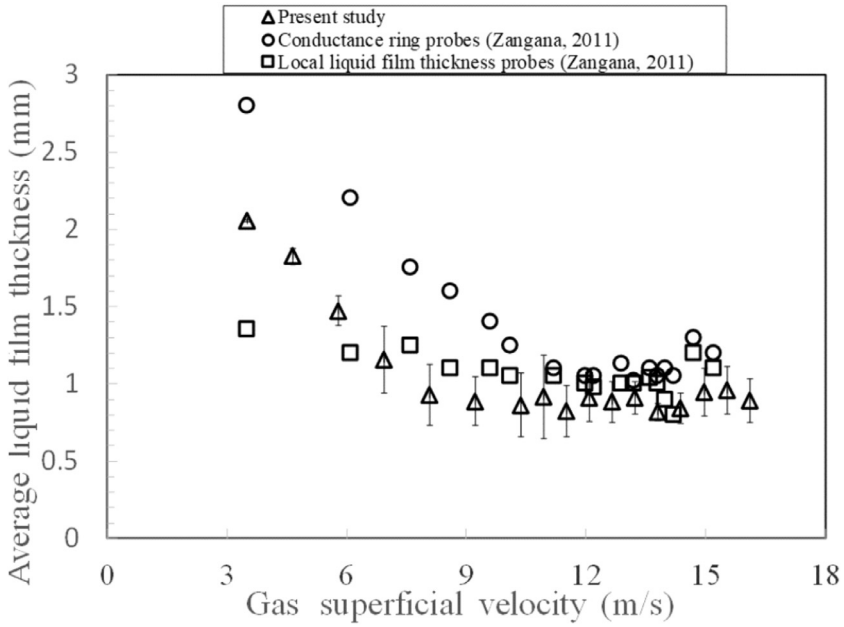

Fig. 9. Comparison of the present work with the conductance ring probe and local film pin probe liquid film thickness at constant liquid and gas superficial velocities of 0.05 and 3.5–15.6 m/s, respectively. The error bar represents standard deviation.

where D is the pipe diameter and is the average void fraction.

From Fig. 8, it can be seen that at liquid superficial velocity ranging from 0.02 to 0.05 m/s, there is a sharp decrease in liquid film thickness as gas superficial velocity is increased up to 9.2 m/s. Beyond this gas superficial velocity, the liquid film thickness is relatively steady up to a gas superficial velocity of about 13.2 m/s. It can be observed that beyond gas superficial velocity of 13.2 m/s, the liquid film thickness increases and then decreases, the sharp increase and decrease could be an indication of a transition point between churn–annular flows. It can be generally observed that the minima in liquid film thickness occur at around gas superficial velocity of around 12.4 m/s. This is in close agreement with the value reported by Van der Meulen (2012). He reported that the general minimum liquid film thickness occurred at gas superficial velocity of 13 m/s using same experimental rig and same conductance ring probes. As expected, the maximum liquid film thickness can be observed at the lowest gas superficial velocity of 3.5 m/s. Fig. 9, on the other hand, shows a comparison of the present work against the results reported by Zangana (2011) using same experimental facility and conductance ring probes but with different local liquid film thickness pin probes at constant liquid superficial velocity of 0.05 m/s.

It can be observed from Fig. 9 that the average values of liquid film thickness from the conductance ring probes are visibly higher at low gas superficial velocity of 3.5 m/s. In contrast, at higher gas superficial velocities 10–16.1 m/s, a reasonably good agreement can be seen from the values of liquid film thickness obtained using the local film pin probes and conductance ring probes. The best explanation for this tendency is that the local pin probes can measure liquid film thickness accurately up to 1.5 mm according to their calibration curves. Therefore, at low gas superficial velocity where the liquid film thickness is expected to be thicker than 1.5 mm, the average values of liquid film thickness obtained locally are lower than those obtained from the conductance ring probes. The observed little difference in conductance ring probe data from the present work and that acquired from Zangana (2011) at lower gas superficial velocity may be attributed to the difference in axial positions from which both conductance ring probe data were gotten.

4.4. Experimental data versus the values from empirical correlations

Chisholm (1972) proposed a correlation for predicting void fraction (Void fraction = 1 – film fraction) using a slip ratio, which was substituted in the homogeneous void fraction equation to obtain void fraction. It is worth mentioning that the Chisholm (1972) correlation was empirically developed for heat exchanger applications. Sixteen years later, Hassan (1988) proposed a correlation for predicting void fraction for churn flows. They achieved this feat by putting into cognisance the fact that an accurate estimate of the flow distribution parameter, C_0, is important for predicting void fraction in churn flow and that the bubble concentration profile is unlikely to be similar to that for slug flows because of the churning motion characteristics of this flow pattern. From their data, they made a linear plot of actual gas velocity, $\frac{U_{SG}}{\varepsilon}$, against mixture velocity, U_m, and obtained a slope which is analogous to C_0 of 1.15. Cioncolini and Thome (2012) developed a correlation for predicting void fraction by incorporating the Hill function. Woldesemayat and Ghajar (2007) studied the performance of 68 void fraction correlations based on 2845 data points. The data set covered a wide range of parameters. They developed a void fraction correlation that they claimed has the best predictive capability of all the correlations considered in their work regardless of flow pattern and pipe inclination angle.

The film fraction correlations proposed by Chisholm (1972), Hassan (1988), Cioncolini and Thome (2012) and Woldesemayat and Ghajar (2007) Eqs. (4), (7), (8) and (11), respectively are as follows:

$$\varepsilon_L = 1 - \varepsilon = \frac{1}{1 + U_R\left(\frac{1-x}{x}\right)\left(\frac{\rho_g}{\rho_l}\right)} \tag{4}$$

where

$$U_R = \frac{U_G}{U_L} = \left[1 - x\left(1 - \frac{\rho_l}{\rho_g}\right)\right]^{0.5} \tag{5}$$

and

$$x = \frac{M_g}{M_g + M_l} = \frac{U_{SG}\rho_g A}{U_{SG}\rho_g A + U_{SL}\rho_l A} = \frac{U_{SG}\rho_g}{U_{SG}\rho_g + U_{SL}\rho_l} \tag{6}$$

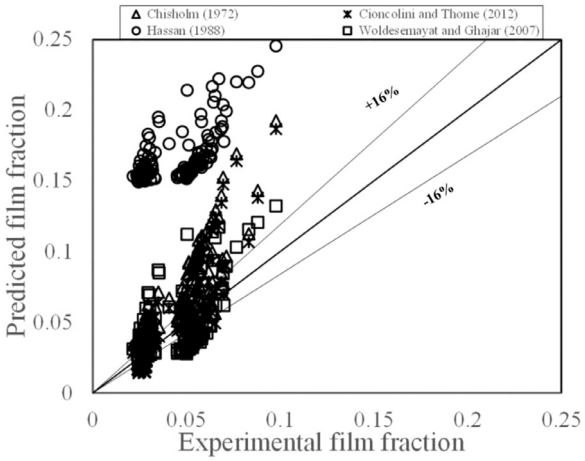

Fig. 10. Comparison between experimental film fraction and calculated film fraction from some empirical models.

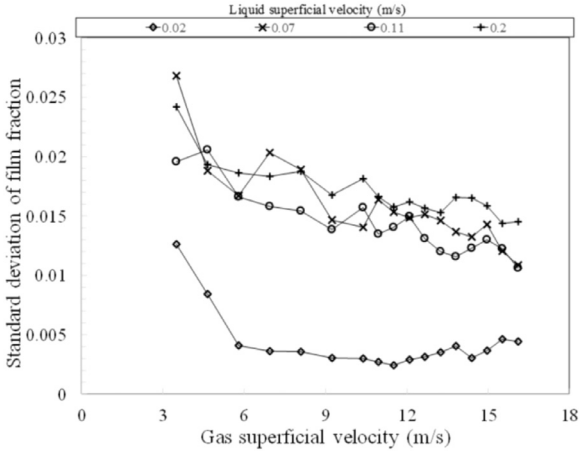

Fig. 11. A plot of variation of standard deviation of film fraction with gas superficial velocity at various liquid superficial velocities. Standard deviation here is the deviation of real film fraction.

$$\varepsilon_L = 1 - \varepsilon = \frac{U_{SG}}{1.15U_m + 0.345\sqrt{\frac{gD}{\rho_l}}(\rho_l - \rho_g)} \tag{7}$$

where $U_m = U_{SG} + U_{SL}$ and U_G and U_L are the actual gas and liquid velocities, respectively.

$$\varepsilon_L = 1 - \varepsilon = \frac{hx^n}{1 + (h-1)x^n}; \quad 0 < x < 1; \quad 10^{-3} < \frac{\rho_l}{\rho_g} < 1; \quad 0.7 < \varepsilon < 1 \tag{8}$$

where

$$h = -2.129 + 3.129\left(\frac{\rho_g}{\rho_l}\right)^{-0.2186} \tag{9}$$

and

$$n = 0.3487 + 0.6513\left(\frac{\rho_g}{\rho_l}\right)^{0.5150} \tag{10}$$

$$\varepsilon_L = 1 - \varepsilon = \frac{U_{SG}}{U_{SG}\left(1 + \left(\frac{U_{SL}}{U_{SG}}\right)\left(\frac{\rho_g}{\rho_l}\right)^{0.1}\right) + 2.9\left(\frac{gD\sigma(1+\cos\theta)(\rho_l - \rho_g)}{{\rho_l}^2}\right)^{0.25}(1.22 + 1.22\sin\theta)\frac{p_{atm}}{p_{sysem}}} \tag{11}$$

where θ is the inclination angle of the pipe, σ is surface tension, p_{atm} and p_{system} are the atmospheric and system pressures, ε is the void fraction and ε_L is film fraction.

Fig. 10 shows a comparison between experimentally determined film fraction against film fraction determined from empirical correlations of Chisholm (1972), Hassan (1988), Cioncolini and Thome (2012) and Woldesemayat and Ghajar (2007). In order to have a better understanding of how each of the 4 published empirical correlations agree well with the present experimental data, a cross-plot is presented in Fig. 10. It can be observed from the figure that the Chisholm (1972) empirical correlation agree reasonably well at low values of experimental film fraction, $E_L \leq 0.1$ and on the other hand fail to predict intermediate film fraction ($0.1 \leq E_L \leq 0.19$) values within $\pm 16\%$. Interestingly, the Cioncolini and Thome (2012) correlation used in predicting film fraction, follows the same trend to the correlation of Chisholm (1972). Since, both correlations were specifically designed for cases where annular flow is the dominant flow pattern. Therefore, both correlations agree well with the data when the liquid superficial velocity is low. This corresponds to film fraction, $\varepsilon_L \leq 0.1$.

The Woldesemayat and Ghajar (2007) does not agree well with the experimental film fraction for $0.08 \leq \varepsilon_L \leq 0.12$.However, the predicted film fraction values begins to agree well with experimental film fraction when $\varepsilon_L \leq 0.08$ within $\pm 16\%$. The correlation is also able to predict film fraction within $\pm 20\%$ for $0.1 \leq \varepsilon_L \leq 0.14$.

On the other hand, Hassan (1988) empirical correlation shows a significant variation with the current data. The disparity could be attributed to two facts namely, (1) the Hassan (1988) empirical model was originally developed for churn flow in smaller diameter pipes and (2) the Hassan (1988) empirical model is a drift flux model which depends on the accuracy of the values of C_0 and the drift velocity (Vgd). The drift velocity on the other hand depends on the drift coefficient (d). The assumed values of C_0 and d are 1.15 and 0.345, respectively, based on his equation may not be appropriate for present work and thus could be responsible for the over-prediction.

In general, the Woldesemayat and Ghajar (2007) shows better prediction capability in comparison to the other three empirical correlations whilst on the other hand, the Hassan (1988) is the poorest.

4.5. Standard deviation (S) of film fraction

In this section, the variation of standard deviation (S) with gas superficial velocity is investigated. The standard deviation is calculated from Eq. (12). Here, S which is the deviation of real film fraction can be used to determine the degree of roughness of film fraction.

$$S = \sqrt{\frac{1}{n}\sum_{i=1}^{n}|\varepsilon_L - \overline{\varepsilon_L}|^2} \tag{12}$$

Fig. 11 shows a plot of variation of S of film fraction time series data with gas superficial velocity at different liquid superficial velocities.

In Fig. 11, a general decreasing trend of averaged S of film fraction with increasing gas superficial velocity can be clearly seen. At low liquid superficial velocity, there is an initial sharp decrease fol-

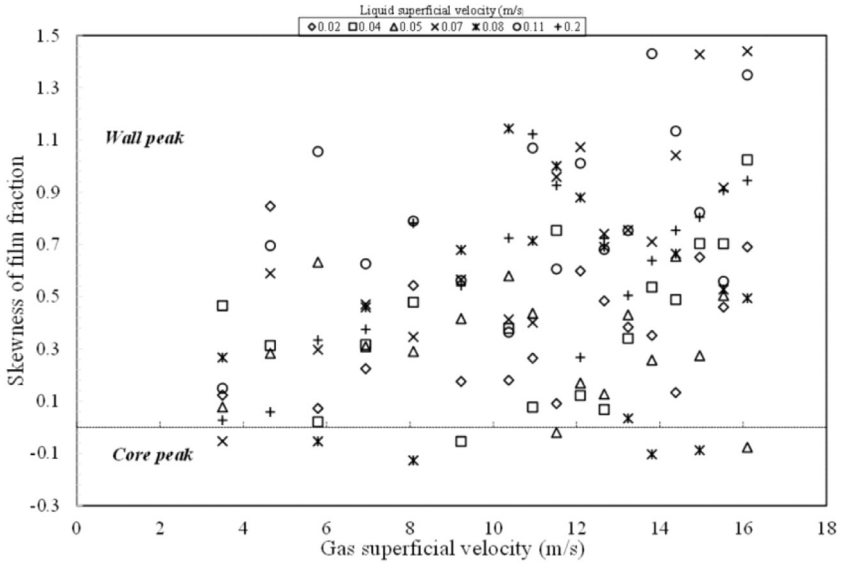

Fig. 12. A plot of variation of skewness of film fraction with gas superficial velocity at various liquid superficial velocities.

lowed by a more or less constant value as the gas superficial velocity increases. This observation could be as a result of more or less steady ripple waves associated with annular flow. As the liquid superficial velocity is increased beyond 0.02 m/s, the flow becomes more oscillatory leading to an alternating increase and decrease as the gas superficial velocity is increased. At liquid superficial velocity of 0.1 m/s, the degree of haphazardness of S of film fraction becomes even more marked. This could be ascribed to churn–annular flow transition boundary.

It can also be seen from Fig. 11 that the peak value of S of film fraction occurs when the liquid superficial velocity is 0.07 m/s. The irregularities in S of film fraction at liquid superficial velocities of 0.07, 0.11 and 0.2 m/s can be attributed to wispy annular flow occurring around the transition point. In wispy annular flow, the gas core contains larger liquid structure compared to the smaller droplets in annular flow.

It can also be observed that the higher values of S occurs at higher liquid superficial velocity and is quite higher than that at low liquid superficial velocity. This is expected because high liquid superficial velocity results in larger liquid film waves which lead to high degree of roughness in the liquid film.

4.6. Skewness of film fraction

Skewness of film fraction (S_k) is used to determine the degree of asymmetry of the gas–liquid flow distribution. For instance, for a bell-shaped probability distribution, S_k will be zero. If there is a shift in the bell-shaped curve to the right, it means that the film fraction is higher and the function gives negative S_k. On the contrary, when there is a shift to the left of the bell-shaped curve, the film fraction is lower, hence the function gives a positive S_k. This parameter has been successfully used by Shen et al. (2005), Qi et al. (2012) and more recently Kanu (2013) to distinguish between core peak and wall peak distribution pattern in two-phase bubbly flow. From their works, they noted that when S_k has negative values, it indicates a core peak phase distribution pattern. A wall peak phase distribution pattern occurs when the skewness is positive. An S_k value of zero represents a transition between the wall peak and core peak phase distribution.

The variation of skewness (S_k) with gas superficial velocity shown in Fig. 12 is investigated. S_k is calculated from Eq. (13). S_k can be used to quantitatively analyse phase distribution in gas–liquid flow.

$$S_k = \frac{\frac{1}{n}\sum_{i=1}^{n}\left|\varepsilon_{L_i} - \overline{\varepsilon_{Li}}\right|^3}{\sigma^3} \tag{13}$$

In Fig. 12, the S_k of film fraction are plotted against gas superficial velocity with liquid superficial velocity as a parameter.

It follows from the explanation given above that as the gas superficial velocity increases, S_k also increases and the phase distribution of the film fraction tends to become more wall peaking or less core peaking.

It can be observed from Fig. 12 that the absolute value of S_k of film fraction is less than 1.5 within the experimental range. It can also be noted that the value of S_k generally increases when the gas superficial velocity is 10.9 m/s within the prevailing liquid superficial velocities considered under this study. This increase in S_k under these conditions may be attributed to a region where transition from churn–annular flow occurred. A general trend in Fig. 12 is that as gas superficial velocity increases, S_k of film fraction and the corresponding phase distribution become more wall peaking and less core peaking.

Since S_k is also dependant on liquid superficial velocity, there is a drift towards core peaking when the liquid superficial velocity is increased at constant gas superficial velocity, this is illustrated in Fig. 13. Fig. 13 shows an increase in S_k when the liquid superficial velocity is less than 0.05 m/s at constant gas superficial velocity. The increase in S_k is particularly most noticeable at low gas superficial velocity. It can also be observed from Fig. 13 that when the liquid superficial velocity is increased beyond 0.05 m/s, S_k shows an alternating increase followed by a decrease.

Since the film fraction shows this clear trend, a more detailed analysis is performed on the time series of film fraction data obtained from the conductance probes.

4.7. Spectral analysis

Spectral analysis of the time series data in the frequency domain has been employed in order to further investigate the periodicity of the interfacial structures. The spectral analysis in form of power spectral density (PSD) is used to quantify the strength of the time series signal across different frequency bands. It is worth mentioning that in the plot of spectrum of auto correlation function, a frequency corresponding to the tallest peak in the plot gives

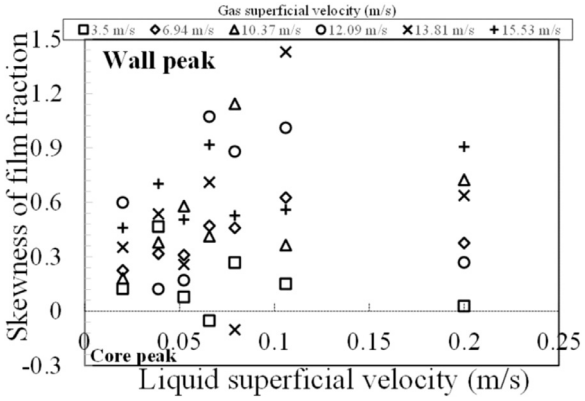

Fig. 13. A plot of variation of skewness of film fraction with liquid superficial velocity at various gas superficial velocities.

the dominant frequency of disturbance waves. Fig. 14 shows the PSD calculated from the film fraction measurements shown in the time series data, Fig. 5. This approach has been used by several previous investigators (Azzopardi, 1986) for calculation of dominant or disturbance wave frequency. Azzopardi (1986) noted that this approach is the most objective approach available for the measurement of disturbance wave frequency.

To obtain the PSD, the Fourier transform of the time series signal is initially carried out and the equation is defined in Kanu (2013):

$$F(x) = \int_{-\infty}^{\infty} \varepsilon_L(t) e^{(-j2\pi ft)dt} \tag{14}$$

The PSD function is then obtained by taking the Fourier transform of the auto covariance function (ACF) as given in Kanu (2013):

$$C_{xx}(k\Delta\tau) = \frac{1}{T-\tau}\int_0^{T-\tau} (\varepsilon_L(t) - \bar{\varepsilon}_L).(\varepsilon_L(t+k\Delta\tau) - \bar{\varepsilon}_L)dt; \;\; \tau < T \tag{15}$$

where T is the duration of sampling, $k\Delta\tau$ is the time delay, τ is the interrogating time delay. The PSD is given by;

$$P_{xx}(f) = \Delta\tau\left(\frac{1}{2}C_{xx}(0) + \sum_{k=1}^{\frac{\tau}{\Delta\tau}-1} C_{xx}(k\Delta\tau)w(k\Delta\tau)\cos(2\pi fk\Delta\tau)\right) \tag{16}$$

In Eq. (16), a cosine windowing function $w(k\Delta\tau)$ is used to suppress the spectrum leakage, Kaji et al. (2009) and Kanu (2013) have also used a similar method, Eq. (17), in their work;

$$w(k\Delta\tau) = cos\left(\frac{\pi k\Delta\tau}{2\tau}\right) \tag{17}$$

Because it is not easy to quantify the effect of variation of frequency on a linear scale, a logarithmic scale is being used on the frequency axis to easily access the effect of frequency and gas superficial velocity variation.

The PSD variation with frequency is shown in Fig. 14 for a constant liquid superficial velocity of 0.33 m/s and at various gas superficial velocities of 6.06–14.2 m/s. The figure shows that at gas superficial velocity of 6.06 m/s, a well-defined peak can be observed. As the gas superficial velocity increases, the profiles remain clearly defined but with the position of frequency shifting to higher frequencies. The peaks decrease by about 66%.

In Fig. 15, dominant frequency obtained from the conductance ring probes is compared against dominant frequency obtained from the work of Sharaf et al. (2016) using wire mesh sensor (WMS) at same liquid and gas superficial velocities. Sharaf et al. (2016) used the same experimental rig as present

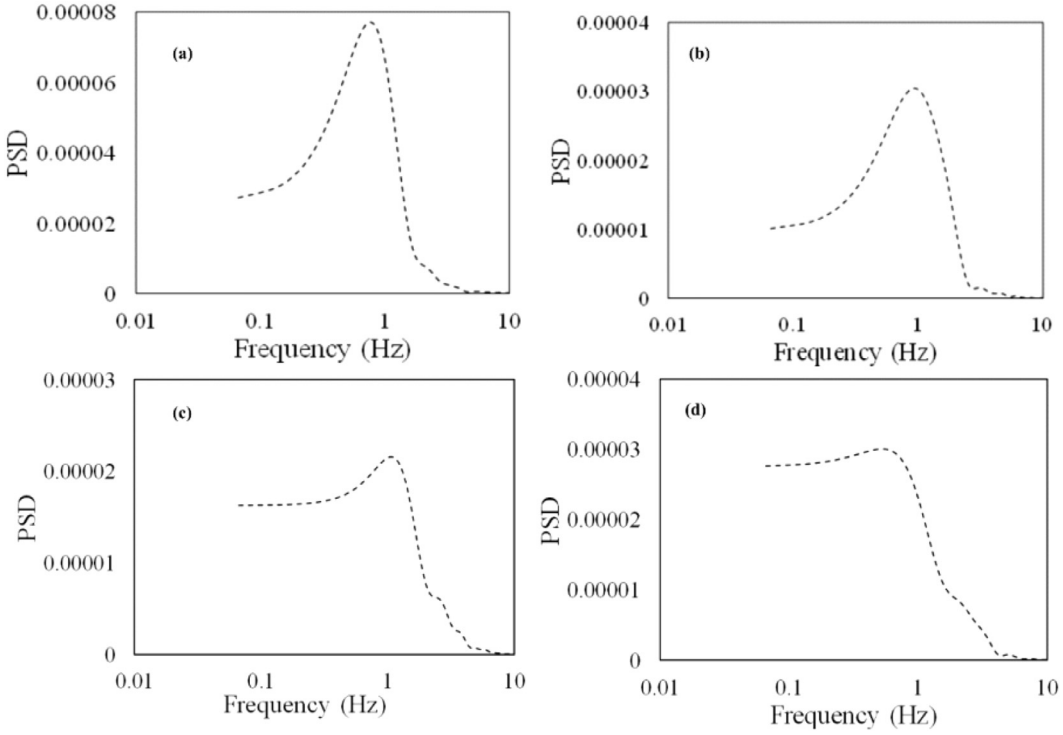

Fig. 14. A plot of variation of Power Spectral Density (PSD) with frequency at constant liquid superficial velocity of 0.33 m/s. Gas superficial velocity (m/s): (a) 6.06 (b) 9.2 (c) 12.7 and (d) 14.2.

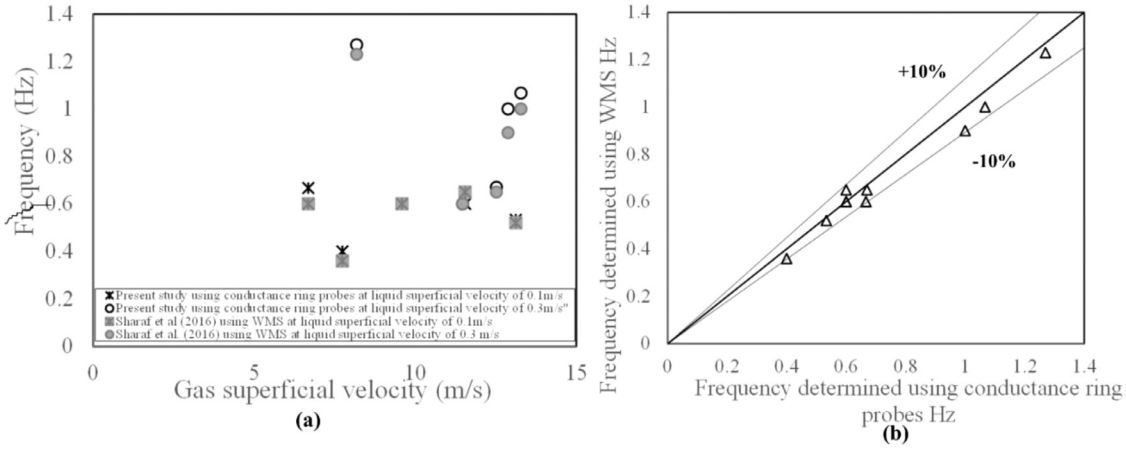

Fig. 15. Comparison of experimentally determined frequency obtained from conductance ring probes and wire mesh sensor (WMS) at various liquid and gas superficial velocities and (b) cross-plot of frequency determined from conductance ring probes and WMS.

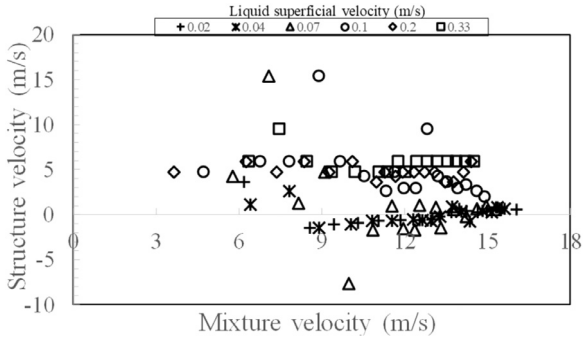

Fig. 16. A plot of variation of structure velocity with mixture velocity at various liquid superficial velocities. (a) Probes 1 and 2 are located at 8.1 and 8.3 m, respectively. Axial distances of 8.1 and 8.3 corresponds to L/D = 64 and 65, respectively.

study, same pipe length and diameter and fluid properties. The sampling frequencies of the conductance ring probes and WMS measurement transducers were 1000 and 1000 Hz, respectively. Fig. 15a shows a plot of average frequency against gas superficial velocity recorded by the conductance ring probes and WMS measurement transducers. The data presented on the figure illustrates good agreement between the two methods of measurements within ±10% as shown in Fig. 15b. Some of the insignificant differences may be due to the fact that the conductance ring probes is not intrusive while the WMS is intrusive.

4.8. Structure velocity

The time series of film fraction is examined further to extract the velocity of periodic structures, also known as structure velocity. Structure velocities from the conductance probes are obtained by cross correlating the signals from the two consecutive axially positioned conductance probes. This technique of structure velocity measurement is objective and it has been utilised by several previous investigators (Nicklin et al., 1962; Azzopardi, 1986; Sawant et al., 2008). Structure velocities for various liquid superficial velocities are plotted against mixture superficial velocity as illustrated in Fig.16.

Fig. 16 shows the variation of structure velocity with mixture velocity in the upstream (between Probes 1 and 2). From the figure, it can be observed that the trend earlier suggested by previous investigators is seen in the present data. Sawant et al. (2008) suggested that in order to increase the accuracy of structure velocity calculation, the two probes should be located as close as possible. It is in view of this recommendation that the probes used in the present work were placed as close as possible to each other.

From Fig. 16, it can be observed that the structure velocity is negative for liquid superficial velocities ranging from 0.02 to 0.07 m/s and at mixture velocities of between 8.8 and 14.5 m/s and become positive at the highest mixture velocities. The change in sign from negative to positive in the value of structure velocity could be as a result of a change in churn to annular flows. This may also imply that there are possible features of counter and co-current flows.

For liquid superficial velocities of 0.1 and 0.33 m/s as depicted in Fig. 16, the structure velocity is almost uniform. This is expected because at high liquid superficial velocities, the disturbance and ripple waves are more uniform. This is in agreement with the conclusions of Azzopardi (1986) that when the waves are very close to each other without coalescence with the successive waves, the structure velocity becomes almost uniform. According to Fukano et al. (1997) the disturbance waves occurring in annular flow become stable as they move along the length of the pipes where the probes are located. The region where there is a decrease in structure velocity could be due to the region where churn flow occurs.

4.9. Comparison between present study and that of Skopich et al. (2015)

A comparison between the present study and that of Skopich et al. (2015) will be made based on average film fractions. Skopich et al. (2015) carried out experimental work on vertical pipe with an internal diameter of 50.8 mm. The fluids employed were air and water at a system pressure of 0.9 bar absolute.

The results of the comparison presented in Fig. 17 were carried out at the same liquid superficial velocity of 0.05 m/s. The plot shows the same tendency, though the values of average film fraction obtained from the work of Skopich et al. (2015) are higher than those of present study. This might be attributed to the fact that the amount of entrainment of liquid drops in the gas core in large diameter pipes is greater than that of smaller pipes. Hence, there is less liquid in the film in the large diameter case.

5. Conclusion

Experimental data are presented and discussed on characteristics of churn and annular air–water flows in an 11 m long riser

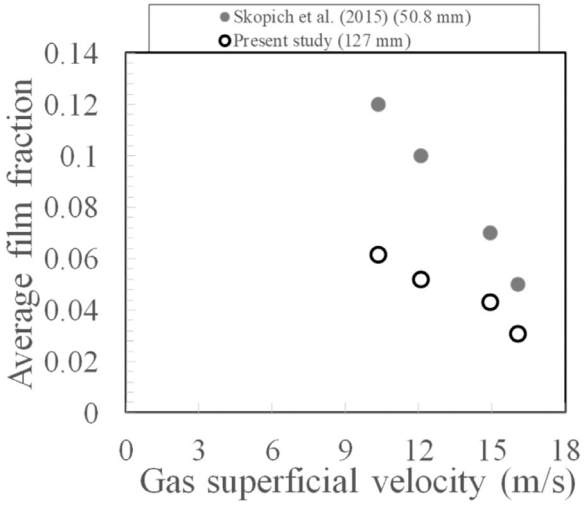

Fig. 17. Comparison of average film fraction (present study) with those of Skopich et al. (2015). Liquid superficial velocity = 0.05 m/s. The comparison is for same liquid and gas superficial velocities. The operating pressure for the work of Skopich et al. (2015) and present study are 0.9 and 3 bars, respectively. The pipe diameter for the work of Skopich et al. (2015) and present study are 50.8 and 127 mm, respectively.

with 127 mm internal diameter using conductance ring probes. The film fraction data obtained from the conductance ring probes were analysed using more objective statistical analysis methods. In the present study only annular and churn flows occurred. Power spectral density (PSD) for each run was examined and plotted against frequency to obtain the dominant frequency. A cross-correlation was performed between the time varying film fraction data measured by the ring probes located at 8.1 and 8.3 m above the mixer section at the base of the riser. This allows the determination of the time for individual waves to travel between every two ring probes, and hence the calculation of the structure velocity. From this data analysis, the following conclusions can be drawn:

- The plot of time series of film fraction at L/D = 64, 65 and 67 showed similar trend and exhibited an insignificant variation in film fraction. The oscillatory nature and high film fraction becomes more evident at low gas superficial velocity of 3.5 m/s. At the highest gas superficial velocity of 16.1 m/s, the peak heights of the film fraction decreases by about 60%.
- The film fraction data from the present work was further compared with that obtained from correlations of proposed by Chisholm (1972), Hassan (1988), Cioncolini and Thome (2012) and Woldesemayat and Ghajar (2007). The result from the comparison indicates that Woldesemayat and Ghajar (2007) correlation performed better than other correlations particularly at lower and intermediate film fraction.
- The results of the comparison of dominant frequency obtained from the conductance ring probes against those obtained from the published work of Sharaf et al. (2016) using wire mesh sensor (WMS) showed good agreement between the two methods of measurements within ± 10%.
- The structure velocity was found to be almost uniform at high liquid superficial velocities. The work also confirms the conclusions of Azzopardi (1997) that disturbance waves become more regular and achieve more uniform velocity when the waves become close to each other without coalescence of the successive waves.
- The comparison between the results of the plot of average film fraction obtained from the present study and those of Skopich et al. (2015) showed the same tendency.

Acknowledgment

Abdulkadir, M., would like to express his sincere appreciation to the Nigerian government through the Petroleum Technology Development Fund (PTDF) for providing the funding for his doctoral studies.

This work has been undertaken within the Joint Project on Transient Multiphase Flows and Flow Assurance. The Author(s) wish to acknowledge the contributions made to this project by the UK Engineering and Physical Sciences Research Council (EPSRC) and the following: GL Industrial Services; BP Exploration; CD-adapco; Chevron; ConocoPhillips; ENI; ExxonMobil; FEESA; IFP; Institutt for Energiteknikk; PDVSA (INTEVEP); Petrobras; PETRONAS; SPT; Shell; SINTEF; Statoil and TOTAL. The Author(s) wish to express their sincere gratitude for this support.

References

Abdulkadir, M., Azzi, A., Zhao, D., Azzopardi, B.J., 2014. Liquid film thickness behaviour within a large diameter vertical 180° return bend. Chem. Eng. Sci. 107, 137–148.
Abdulkadir, M., Zhao, D., Azzi, A.L., Lowndes, I.S., Azzopardi, B.J., 2012. Two-phase air–water flow through a large diameter vertical 180° return bend. Chem. Eng. Sci. 79, 138–152.
Ali, S.F., 2009. Two-Phase Flow In Large Diameter Vertical Pipes PhD thesis. Cranfield University.
Almabrok, A., 2013. Gas–Liquid Two-Phase Flow In Up And Down Vertical Pipes PhD thesis. Cranfield University.
Ansari, A.M., Sylvester, N.D., Sarica, C., Shoham, O., Brill, J.P., 1994. A comprehensive mechanistic model for upward two-phase flow in wellbores. Soc. Pet. Eng. Prod. Facil. 9, 143–152.
Azzopardi, B.J., 1986. Disturbance wave frequencies, velocities and spacing in vertical annular two-phase flow. Nucl Eng Des 92, 121–133.
Azzopardi, B.J., 1997. Drops in annular two-phase flow. Int. J. Multiph. Flow 23, 1–53.
Azzopardi, B.J., Wren, E., 2004. What is entrainment in vertical two-phase churn flow? Int. J. Multiph. Flow 30, 89–103.
Barbosa, J.R., Govan, A.H., Hewitt, G.F., 2001. Visualization and modelling studies of churn flow in a vertical pipe. Int. J. Multiph. Flow 27, 2105–2127.
Barnea, D., 1987. A unified model for predicting flow pattern transitions for the whole range of pipe inclinations. Int. J. Multiph. Flow 13, 1–12.
Brown, D.J., Jensen, A., Whalley, P.B., 1975. Non-equilibrium effects in heated and unheated annular two-phase flow. ASME Paper 75, 754–757.
Chisholm, D., 1972. An equation for velocity ratio in two-phase flow. N. E. E. Report, No. 535.
Cioncolini, A., Thome, J.R., 2012. Void fraction prediction in annular two-phase flow. Int. J. Multiph. Flow 43, 72–84.
Da Riva, E., Del Col, D., 2009. Numerical simulation of churn flow in a vertical pipe. Chem. Eng. Sci. 64, 3753–3765.
Dukler, A.E., Taitel, Y., 1986. Flow pattern transition in gas–liquid systems: measurement and modelling. Multiph. Sci. Meas. 2, 1–94.
Fossa, M., 1998. Design and performance of a conductance probe for measuring the liquid fraction in two-phase gas-liquid flows. Flow Meas. Instrum. 9, 103–109.
Fukano, T., Nakagawa, H., Mori, Y., Watanabe, M., 1997. Liquid film formation on the inner surface of the horizontal channel. Nucl. Eng. Des. 175, 3–13.
Govier, G.W., Aziz, K., 1972. Flow of Complex Mixtures in Pipes. Van-Nostrand-Reinhold, Princeton, New Jersey, USA.
Hassan, A.R., 1988. Void fraction in bubbly, slug and churn flow in vertical two-phase up-flow. Chem. Eng. Commun. 66, 101–111.
Hawkes, N.J., Lawrence, C.J., Hewitt, G.F., 2000. Studies of annular–wispy flow using transient pressure gradient and optical measurements. Int. J. Multiph. Flow 26, 1565–1582.
Hazuku, T., Takamasa, T., Matsumoto, Y., 2008. Experimental study on axial development of liquid film in vertical upward annular two-phase flow. Int. J. Multiph. Flow 34, 111–127.
Hewitt, G.F., Jayanti, S., 1993. To churn or not to churn. Int. J. Multiph. Flow 19, 527–529.
Hewitt, G.F., Martin, C.J., Wilkes, N.S., 1985. Experiental and modelling studies of annular flow in the region between flow reversal and the pressure drop minimum. Phys. Chem. Hydrodyn. 6, 69–86.
Jayanti, S., Hewitt, G.F., 1992. Prediction of the slug-to-churn flow transition in vertical two-phase flow. Int. J. Multiph. Flow 18, 847–860.
Jayanti, S., Hewitt, G.F., Low, D.E.F., Hervieu, E., 1993. Observation of flooding in the Taylor bubble of co-current upwards slug flow. Int. J. Multiph. Flow 19, 531–534.
Julia, J.E., Ozar, B., Dixit, A., Jeong, J.J., Hibiki, T., Ishii, M., 2009. Axial flow development of flow regime in adiabatic upward two-phase flow in a vertical annulus. J. Fluids Eng.-T ASME 131, 0213021–02130211.
Kaji, R., Azzopardi, B.J., 2010. The effect of pipe diameter on the structure of gas/liquid flow in vertical pipes. Int. J. Multiph. Flow 36, 303–313.
Kaji, R., Azzopardi, B.J., Lucas, D., 2009. Investigation of flow development of co-current gas–liquid vertical slug flow. Int. J. Multiph. Flow 35, 335–348.

Kanu, U.O.A, 2013. Characterisation of Churn Flow Coalescers (CFC) in Vertical Pipes PhD thesis. University of Nottingham.
Kataoka, I., Ishii, M., 1987. Drift flux model for large diameter pipe and new correlations for pool void fraction. Int. J. Heat Mass Transf. 30, 1927–1939.
Mao, Z.S., Dukler, A.E., 1993. Brief communication: the myth of churn flow. Int. J. Multiph. Flow 19, 377–383.
Mishima, K., Ishii, M., 1984. Flow regime transition criteria for upward two-phase flow in vertical tubes. Int. J. Heat Mass Transf. 27, 723–737.
Nicklin, D.J., Wilkes, J.O., Davidson, J.F., 1962. Two-phase flow in vertical tubes. Trans. Instit. Chem. Eng. 156, 61–68.
Ohnuki, A., Akimoto, H., Sudo, Y., 1995. Flow pattern and its transitions in gas–liquid two phase flow along as large vertical pipe. In: Proceedings of the 2nd International Conference on Multiphase Flow. Kyoto, Japan.
Omebere-Iyari, N.K., 2006. The Effect Of Pipe Diameter And Pressure In Vertical Two-Phase Flow PhD Thesis. University of Nottingham.
Omebere-Iyari, N.K., Azzopardi, B.J., 2007. Two-phase flow patterns in large diameter vertical pipes at high pressures. AIChE 53, 2493–2504.
Oshinowo, T., Charles, M.E., 1974. Vertical two-phase flow- Part 1: flow pattern correlations. Can. J. Chem. Eng. 52, 25–35.
Pereyra, E., Torres, C., 2005. FLOPATN—Flow Pattern Prediction and Plotting Computer Code. The University of Tulsa, Tulsa, Oklahoma, USA.
Qi, F.S., Yeoh, G.H., Cheung, S.C.P., Tu, J.Y., Krepper, E., Lucas, D., 2012. Classification of bubbles in vertical gas–liquid flow: part 1—analysis of experimental data. Int. J. Multiph. Flow 39, 121–134.
Sawant, P.H., Ishii, M., Mori, M., 2008. Prediction of amount of entrained droplets in vertical annular two-phase flow. Int. J. Heat Fluid Flow 30, 715–728.
Sekoguchi, K., Takeishi, M, 1989. Interfacial structure in upward huge wave flow and annular flow regimes. Int. J. Multiph. Flow 15, 295–305.
Sharaf, S., van der Meulen, P., Agunlejika, E.O., Azzopardi, B.J., 2016. Structures in gas–liquid churn flow in large diameter pipe. Int. J. Multiph. Flow 78, 88–103.
Shen, X., Mishima, K., Nakamura, H., 2005. Two-phase distribution in vertical large diameter pipe. Int. J. Heat Mass Transf. 48, 211–225.
Shoham, O., 2006. Mechanistic Modelling of Gas–Liquid Two-Phase Flow in Pipes. University of Tulsa, Society of Petroleum Engineers, USA.
Skopich, A., Pereyra, E., Sarica, C., Kelkar, M., 2015. Pipe diameter effect on liquid loading in vertical gas wells. SPE Product. Oper. 30, 164–176.
SPE, 2015. Society of Petroleum Engineers Technical Report. SPE, Richardson.
Taitel, Y., Barnea, D., Dukler, A.E., 1980. Modelling flow pattern transitions for steady upward gas-liquid flow in vertical tubes. AIChE J. 26, 345–354.
Van der Meulen, G.P., 2012. Churn–Annular Gas–Liquid Flows In Large Diameter Vertical Pipes PhD thesis. University of Nottingham.
Van Hout, R., Barnea, D., Shemer, L., 2001. Evolution of statistical parameters of gas–liquid slug flow along vertical pipes. Int. J. Multiph. Flow 27, 1579–1602.
Waltrich, P.J., Falcone, G., Barbosa, J.R., 2013. Axial development of annular, churn and slug flows in a vertical tube. Int. J. Multiph. Flow 57, 38–48.
Wang, K., Bai, B., Cui, J., Ma, W., 2012. A physical model for huge wave movement in gas–liquid churn flow. Chem. Eng. Sci. 79, 19–28.
Wang, K., Bai, B., Ma, W., 2013. Huge wave and drop entrainment mechanism in gas–liquid churn flow. Chem. Eng. Sci. 104, 638–646.
Woldesemayat, M.A., Ghajar, A.J., 2007. Comparison of void fraction correlations for different flow patterns in horizontal and upward inclined pipes. Int. J. Multiph. Flow 33, 347–370.
Wolf, A., Jayanti, S., Hewitt, G.F., 2001. Flow development in vertical annular flow. Chem. Eng. Sci. 56, 3221–3235.
Zabaras, G., Menson, R., Schoppa, W., Wicks III, M., 2013. Large diameter riser laboratory gas–lift tests. Offshore Technology Conference. Houston, Texas, 6–9 May.
Zangana, M.H.S., 2011. Film Behaviour Of Vertical Gas–Liquid Flow In A Large Diameter Pipe PhD thesis. University of Nottingham.